PHYSICAL REVIEW D **72,** 114507 (2005)

1^{-+} exotic meson at light quark masses

J. N. Hedditch, W. Kamleh, B. G. Lasscock, D. B. Leinweber, and A. G. Williams
Department of Physics and Mathematical Physics and Special Research Centre for the Subatomic Structure of Matter, University of Adelaide, 5005, Australia

J. M. Zanotti
John von Neumann-Institut für Computing NIC, Deutches Elektronen-Synchrotron DESY, D-15738 Zeuthen, Germany
(Received 23 September 2005; published 16 December 2005)

The mass of the 1^{-+} exotic meson, created with hybrid interpolating fields, is explored in numerical simulations of quenched QCD on large ($20^3 \times 40$) lattices to obtain good control of statistical and finite volume errors. Using the Fat-Link Irrelevant Clover (FLIC) fermion action, the properties of the 1^{-+} are investigated at light quark masses approaching 25 MeV ($m_\pi/m_\rho \simeq 1/3$). Under the standard assumption that the coupling to the quenched $a_1\eta'$ channel comes with a negative metric, our results indicate that the 1^{-+} exotic exhibits significant curvature close to the chiral limit, suggesting previous linear extrapolations have overestimated the mass of the 1^{-+}. We find for the first time in lattice studies a 1^{-+} mass consistent with the $\pi_1(1600)$ candidate. We also find a strangeness ± 1 $J^P = 1^-$ state with a mass close to 2 GeV.

DOI: 10.1103/PhysRevD.72.114507 PACS numbers: 11.15.Ha, 12.38.Gc, 14.40.Cs

I. INTRODUCTION

The masses of the so-called 'exotic' mesons are attracting considerable attention from the experimental community [1–8] as a vehicle for the elucidation of the relatively unexplored role of gluons in QCD. The Particle Data Group [9] reports two candidates for the 1^{-+} exotic, the $\pi_1(1400)$ at 1.376(17) GeV, and the $\pi_1(1600)$ at 1.596^{+25}_{-14} GeV. The experimental status of these states is an issue that continues to attract attention [6,7].

Lattice QCD provides a first principles approach to nonperturbative calculations of QCD, indispensable in determining the hadron mass spectrum. In the early work of Ref. [10], the UKQCD Collaboration made use of gauge-invariant nonlocal operators to explore P and D-wave mesons, as well as exotics. They used a tadpole-improved clover action, with 375 configurations on a $16^3 \times 48$ lattice. Their calculation was performed at a single quark mass corresponding to approximately that of the strange quark and reported a 1^{-+} exotic mass of 1.9(4) GeV.

In 1997, the MILC Collaboration used local operators formed by combining the gluon field strength tensor and standard quark bilinears [11], the same approach we take in this paper. The highly anisotropic lattices employed allowed many time slices to be used in determining the mass of the exotic. $20^3 \times 48$ and $32^3 \times 64$ lattices with multiple fermion sources per lattice were considered. Using the Wilson action, they suggested a 1^{-+} mass of 1.97(9) GeV from a linear extrapolation in $1/\kappa$ from $m_\pi^2 \geq 0.64$ GeV.

The SESAM Collaboration [12] analyzed dynamical fermion configurations at four quark masses corresponding to $m_\pi^2 \geq 0.455(9)$ GeV^2. Their linear extrapolation resulted in 1.9(2) GeV for the mass of the 1^{-+} exotic where the scale was determined via the Sommer parameter [13] r_0 via Ref. [14].

Further work using the Clover action, but this time with local interpolators was performed by Mei *et al.* in Ref. [15]. Very heavy quark masses were used to get good control of statistical errors. Their linear extrapolation from $m_\pi^2 \geq 1.05$ GeV^2 suggested a mass of 2.01(7) GeV.

In 2002 the MILC Collaboration published new work [16] using dynamical improved Kogut-Susskind fermions on $20^3 \times 48$ and $32^3 \times 64$ lattices. Linearly extrapolating from $m_\pi^2 \geq 0.488$ GeV^2, Bernard *et al.* quote two sets of results for the 1^{-+} mass. Using $r_1 = 0.34$ fm and $\sqrt{\sigma} = 440$ MeV they report a 1^{-+} mass of 1.85(7) and 2.03(7) GeV, respectively.

Michael [17] provides a good summary of work to 2003, concluding that the light quark exotic is predicted by lattice studies to have a mass of 1.9(2) GeV.

In order to minimize the need for extrapolation one requires access to quark masses near the chiral regime on large physical volumes. Our study considers a physical volume of (2.6 fm)^3, and the $\mathcal{O}(a)$-improved FLIC fermion action [18–20] whose improved chiral properties [21] permit the use of very light quark masses which are key to our results.

II. VECTOR MESONS ON THE LATTICE

Consider the momentum-space meson two-point function for $t > 0$,

$$G^{ij}_{\mu\nu}(t, \vec{p}) = \sum_{\vec{x}} e^{-i\vec{p}\cdot\vec{x}} \langle \Omega | \chi^i_\mu(t, \vec{x}) \chi^{j\dagger}_\nu(0, \vec{0}) | \Omega \rangle \quad (1)$$

where i, j label the different interpolating fields and μ, ν label the Lorentz indices. At the hadronic level,

$$G^{ij}_{\mu\nu}(t, \vec{p}) = \sum_{\vec{x}} e^{-i\vec{p}\cdot\vec{x}} \sum_{E, \vec{p}', s} \langle \Omega | \chi^i_\mu(t, \vec{x}) | E, \vec{p}', s \rangle \times \langle E, \vec{p}', s | \chi^{j\dagger}_\nu(0, \vec{0}) | \Omega \rangle$$

where the $|E, \vec{p}', s\rangle$ are a complete set of hadronic states, of energy E, momentum $\vec{p}'$, and spin s,

$$\sum_{E,\vec{p}',s} |E, \vec{p}', s\rangle\langle E, \vec{p}', s| = I. \tag{2}$$

We denote the vacuum couplings as follows:

$$\langle\Omega|\chi^i_\mu|E, \vec{p}', s\rangle = \lambda^i_E \epsilon_\mu(p', s),$$
$$\langle E, \vec{p}', s|\chi^{j\dagger}_\nu|\Omega\rangle = \lambda^{j\star}_E \epsilon^\star_\nu(p', s),$$

where the four-vector $p' = (E, \vec{p}')$ is introduced.

We can translate the sink operator from x to 0 to write this as

$$\sum_{\vec{x},E,\vec{p}',s} e^{-i\vec{p}\cdot\vec{x}}\langle\Omega|\chi^i_\mu(0)e^{i\hat{\vec{P}}\cdot\vec{x}-\hat{H}t}|E, \vec{p}', s\rangle\langle E, \vec{p}', s|\chi^{j\dagger}_\nu(0)|\Omega\rangle$$
$$= \sum_{E,s} e^{-Et}\langle\Omega|\chi^i_\mu|E, \vec{p}, s\rangle\langle E, \vec{p}, s|\chi^{j\dagger}_\mu|\Omega\rangle$$
$$= \sum_{E,s} e^{-Et}\lambda^i\epsilon_\mu(p, s)\lambda^{j\star}\epsilon^\star_\nu(p, s).$$

We shall label the states which have the χ interpolating field quantum numbers as $|\alpha\rangle$ for $\alpha = 1, 2, \cdots, N$, thus replacing $\sum_E$ with $\sum_\alpha$. In general the number of states, N, in this tower of excited states may be very large, but we will only ever need to consider a finite set of the lowest energy states here, as higher states will be exponentially suppressed as we evolve to large Euclidean time. Finally, the transversality condition:

$$\sum_s \epsilon_\mu(p, s)\epsilon^\star_\nu(p, s) = -\left(g_{\mu\nu} - \frac{p_\mu p_\nu}{m^2}\right) \tag{4}$$

implies that for $\vec{p} = 0$, we have

$$G^{ij}_{00}(t, \vec{0}) = 0, \qquad G^{ij}_{kl}(t, \vec{0}) = \sum_\alpha \delta_{kl}\lambda^i_\alpha\lambda^{j\star}_\alpha e^{-m_\alpha t}. \tag{5}$$

Since G^{ij}_{11}, G^{ij}_{22}, and G^{ij}_{33} are all estimates for the same quantity we add them together to reduce variance, forming the sum

$$G^{ij} = G^{ij}_{11} + G^{ij}_{22} + G^{ij}_{33}.$$

Evolving to large Euclidean time will suppress higher mass states exponentially with respect to the lowest-lying state, leading to the following definition of the effective mass

$$M^{ij}_{\text{eff}}(t) = \ln\left(\frac{G^{ij}(t, \vec{0})}{G^{ij}(t+1, \vec{0})}\right). \tag{6}$$

The presence of a plateau in M_{eff} as a function of time, then, signals that only the ground-state signal remains.

III. LATTICE SIMULATIONS

A. Interpolating fields

The formulation of effective interpolating fields for the creation and annihilation of exotic meson states continues to be an active area of research. For example, one can generalize the structure of the interpolating fields to include nonlocal components where link paths are incorporated to maintain gauge invariance and carry the nontrivial quantum numbers of the gluon fields [10,12]. In this case, numerous quark propagators are required for each gauge-field configuration rendering the approach computationally expensive. The use of nonlocal interpolating fields affords greater freedom in creation of operators and facilitates access to exited states through variational techniques, but does not lead to an increase in signal for the ground state 1^{-+} exotic commensurate with the increased computational cost of this approach. Exotic quantum numbers may also be obtained from four-quark ($q\bar{q}q\bar{q}$) operators, but in practice, these tend to exhibit larger statistical fluctuations [10–12].

We consider the local interpolating fields summarized in Table I. Gauge-invariant Gaussian smearing [22,23] is applied at the fermion source ($t = 8$), and local sinks are used to maintain strong signal in the two-point correlation functions. Chromoelectric and magnetic fields are created from 3D APE-smeared links [24] at both the source and sink using the highly improved $\mathcal{O}(a^4)$-improved lattice field strength tensor [25] described in greater detail below.

While all four 1^{-+} interpolating fields of Table I have been used to create the 1^{-+} state on the lattice, in this work we will focus on the results for the two 1^{-+} interpolating fields coupling large spinor components to large spinor components:

$$\chi_2 = i\epsilon_{jkl}\bar{q}^a\gamma_k B^{ab}_l q^b, \qquad \chi_3 = i\epsilon_{jkl}\bar{q}^a\gamma_4\gamma_k B^{ab}_l q^b. \tag{7}$$

TABLE I. J^{PC} quantum numbers and their associated meson interpolating fields.

0^{++}	0^{+-}	0^{-+}	0^{--}	1^{++}	1^{+-}	1^{-+}	1^{--}
$\bar{q}^a q^a$	$i\bar{q}^a\gamma_5\gamma_j B^{ab}_j q^b$	$\bar{q}^a\gamma_5 q^a$	$\bar{q}^a\gamma_5\gamma_j E^{ab}_j q^b$	$\bar{q}^a\gamma_5\gamma_j q^a$	$\bar{q}^a\gamma_5\gamma_4\gamma_j q^a$	$\bar{q}^a\gamma_4 E^{ab}_j q^b$	$i\bar{q}^a\gamma_5 B^{ab}_j q^b$
$\bar{q}^a\gamma_j E^{ab}_j q^b$	$\bar{q}^a\gamma_4 q^a$	$\bar{q}^a\gamma_5\gamma_4 q^a$		$i\bar{q}^a\gamma_4 B^{ab}_j q^b$	$\bar{q}^a\gamma_5\gamma_4 E^{ab}_j q^b$	$i\epsilon_{jkl}\bar{q}^a\gamma_k B^{ab}_l q^b$	$\bar{q}^a\gamma_4\gamma_j q^a$
$i\bar{q}^a\gamma_j\gamma_4\gamma_5 B^{ab}_j q^b$		$i\bar{q}^a\gamma_j B^{ab}_j q^b$		$\epsilon_{jkl}\bar{q}^a\gamma_k E^{ab}_l q^b$	$\bar{q}^a\gamma_5 E^{ab}_j q^b$	$i\epsilon_{jkl}\bar{q}^a\gamma_4\gamma_k B^{ab}_l q^b$	$\bar{q}^a E^{ab}_j q^b$
$\bar{q}^a\gamma_j\gamma_4 E^{ab}_j q^b$		$i\bar{q}^a\gamma_4\gamma_j B^{ab}_j q^b$		$\epsilon_{jkl}\bar{q}^a\gamma_k\gamma_4 E^{ab}_l q^b$	$i\bar{q}^a B^{ab}_j q^b$	$\epsilon_{jkl}\bar{q}^a\gamma_5\gamma_4\gamma_k E^{ab}_l q^b$	$\bar{q}^a\gamma_j q^a$
							$i\bar{q}^a\gamma_4\gamma_5 B^{ab}_j q^b$

These interpolating fields provide the strongest signal for the 1^{-+} state. In both fields the gluonic component is contributing axial-vector quantum numbers.

B. Lattice field strength tensor

In order to obtain the chromoelectric and chromomagnetic fields with which we build the hybrid operators, we make use of a modified version of APE smearing, in which the smeared links do not involve averages which include links in the temporal direction. In this way we preserve the notion of a Euclidean "time" and avoid overlap of the creation and annihilation operators.

In this study, the smearing fraction $\alpha = 0.7$ (keeping 0.3 of the original link) and the process of smearing and SU(3) link projection is iterated 6 times [26]. Each iteration of our modified APE-smearing algorithm proceeds as

$$U_i(x) \rightarrow (1-\alpha)U_i(x) + \frac{\alpha}{4}\sum_{j=1}^{3}(1-\delta_{ij})U_j(x)U_i(x+\hat{j})U_j^\dagger(x+\hat{i}) + \frac{\alpha}{4}\sum_{j=1}^{3}(1-\delta_{ij})U_j^\dagger(x-\hat{j})U_i(x-\hat{j})U_j(x-\hat{j}+\hat{i}),$$

$$U_4(x) \rightarrow (1-\alpha)U_4(x) + \frac{\alpha}{6}\sum_{j=1}^{3}U_j(x)U_4(x+\hat{j})U_j^\dagger(x+\hat{4}) + \frac{\alpha}{6}\sum_{j=1}^{3}U_j^\dagger(x-\hat{j})U_4(x-\hat{j})U_j(x-\hat{j}+\hat{4}).$$

Smearing the links permits the use of highly improved definitions of the lattice field strength tensor, from which our hybrid operators are derived. Details of the $\mathcal{O}(a^4)$-improved tensor are given in [25]. This amount of smearing is suitable for the creation of exotic mesons.

C. Fat-link irrelevant fermion action

Propagators are generated using the fat-link irrelevant clover (FLIC) fermion action [18] where the irrelevant Wilson and clover terms of the fermion action are constructed using fat links, while the relevant operators use the untouched (thin) gauge links. Fat links are created via APE smearing [24]. In the FLIC action, this reduces the problem of exceptional configurations encountered with clover actions [21], and minimizes the effect of renormalization on the action improvement terms [27]. Access to the light quark mass regime is enabled by the improved chiral properties of the lattice fermion action [21]. By smearing only the irrelevant, higher dimensional terms in the action, and leaving the relevant dimension four operators untouched, short distance quark and gluon interactions are retained. Details of this approach may be found in Ref. [18]. FLIC fermions provide a new form of nonperturbative $\mathcal{O}(a)$ improvement [21,27] where near-continuum results are obtained at finite lattice spacing.

D. Gauge action

We use quenched-QCD gauge fields created by the CSSM Lattice Collaboration with the $\mathcal{O}(a^2)$ mean-field improved Lüscher-Weisz plaquette plus rectangle gauge action [28] using the plaquette measure for the mean link. The gauge-field parameters are defined by

$$S_G = \frac{5\beta}{3}\sum_{\substack{x\mu\nu\\ \nu>\mu}}\frac{1}{3}\mathrm{Re\,Tr}(1-P_{\mu\nu}(x)) - \frac{\beta}{12u_0^2}\sum_{\substack{x\mu\nu\\ \nu>\mu}}\frac{1}{3}\mathrm{Re\,Tr}(2-R_{\mu\nu}(x)),$$

where $P_{\mu\nu}$ and $R_{\mu\nu}$ are defined in the usual manner and the link product $R_{\mu\nu}$ contains the sum of the rectangular 1×2 and 2×1 Wilson loops.

The CSSM configurations are generated using the Cabibbo-Marinari pseudo-heat-bath algorithm [29] using a parallel algorithm with appropriate link partitioning [30]. To improve the ergodicity of the Markov chain process, the three diagonal SU(2) subgroups of SU(3) are looped over twice [31] and a parity transformation [32] is applied randomly to each gauge-field configuration saved during the Markov chain process.

E. Simulation parameters

The calculations of meson masses are performed on $20^3\times 40$ lattices at $\beta = 4.53$, which provides a lattice spacing of $a = 0.128(2)$ fm set by the Sommer parameter $r_0 = 0.49$ fm.

A fixed boundary condition in the time direction is used for the fermions by setting $U_t(\vec{x}, N_t) = 0\forall\vec{x}$ in the hopping terms of the fermion action, with periodic boundary conditions imposed in the spatial directions.

Eight quark masses are considered in the calculations and the strange quark mass is taken to be the third heaviest quark mass. This provides a pseudoscalar mass of 697 MeV which compares well with the experimental value of $(2M_K^2 - M_\pi^2)^{1/2} = 693$ MeV motivated by leading order chiral perturbation theory.

The analysis is based on a sample of 345 configurations, and the error analysis is performed by a third-order single-elimination jackknife, with the χ^2 per degree of freedom (χ^2/dof) obtained via covariance matrix fits.

IV. RESULTS

Figures 1 and 2 show the natural log of the correlation functions calculated with interpolators χ_2 and χ_3 from Eq. (7), respectively. The curves become linear after two time slices from the source, corresponding to approxi-

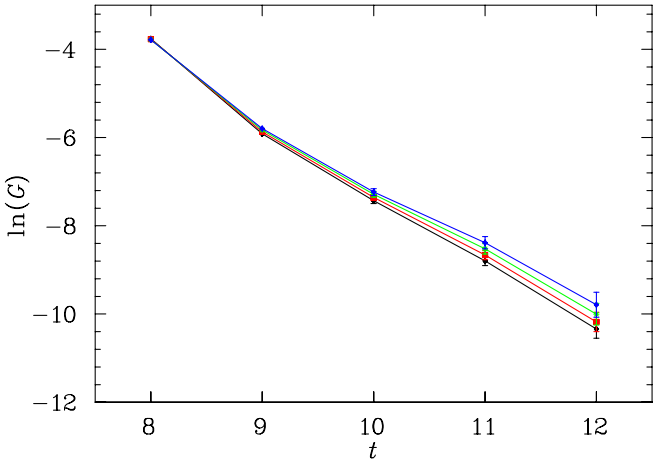

FIG. 1 (color online). Exotic meson propagator for interpolator χ_2. Results are shown for every 2nd quark mass in the simulation. Lower lines correspond to heavier quark masses. For all but the heaviest mass, the signal is lost after $t = 12$.

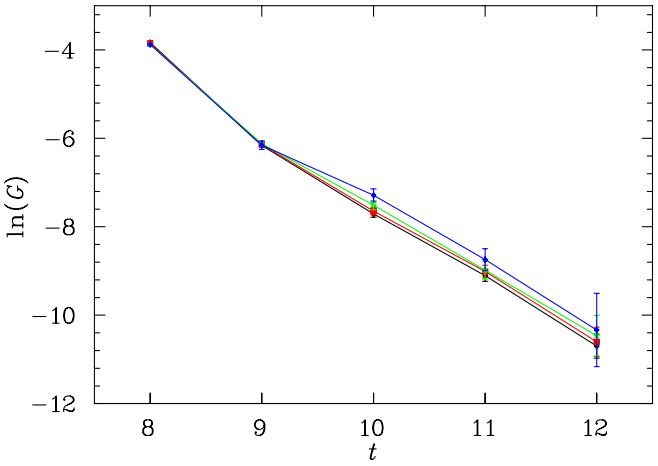

FIG. 2 (color online). Exotic meson propagator for interpolator χ_3. Results are shown for every 2nd quark mass in the simulation. Lower lines correspond to heavier quark masses.

mately 0.256 fm. This is consistent with Ref. [11], where a similar effect is seen after approximately 3 to 4 time slices, corresponding to 0.21 to 0.28 fm following the source.

Figures 3 and 4 show the effective mass for the two different interpolators. For clarity, we have plotted the results for every second quark mass used in our simulation. The plateaus demonstrate that we do indeed see an exotic signal in quenched lattice QCD. This is significant, as we expect the two interpolating fields to possess considerably different excited-state contributions, based on experience with pseudoscalar interpolators [33].

For example, the approach to the pion-mass plateau is from above (below) for the pseudoscalar (axial-vector) interpolating field as illustrated in Fig. 5 (Fig. 6). This exhibits the very different overlap of the interpolators with excited states. As in the 1^{-+} interpolators, the role

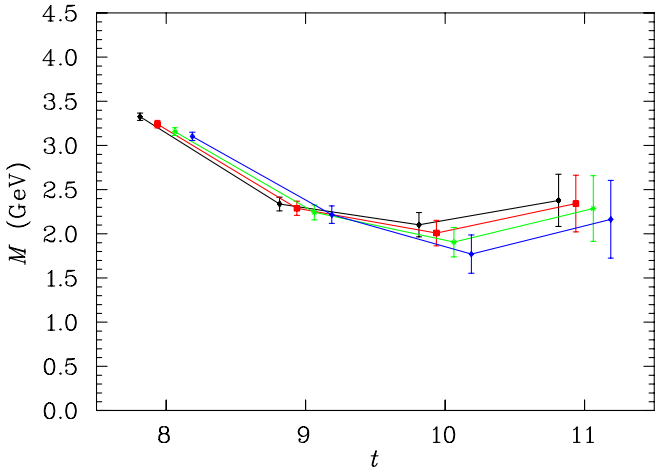

FIG. 3 (color online). Effective mass for interpolator χ_2. Plot symbols are as for the corresponding propagator plot.

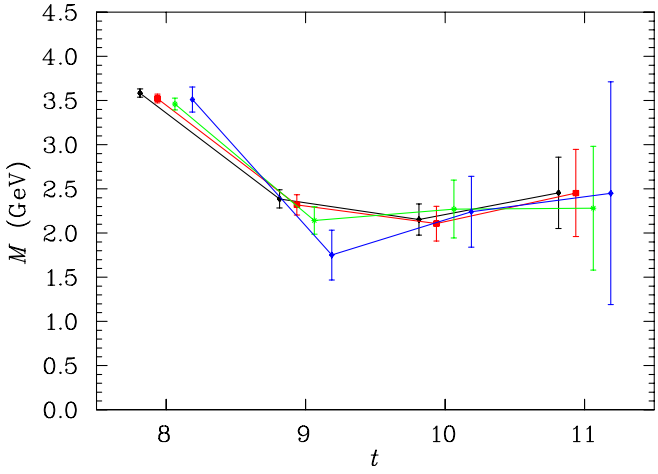

FIG. 4 (color online). As for Fig. 3, but for interpolator χ_3. Signal is lost after $t = 11$.

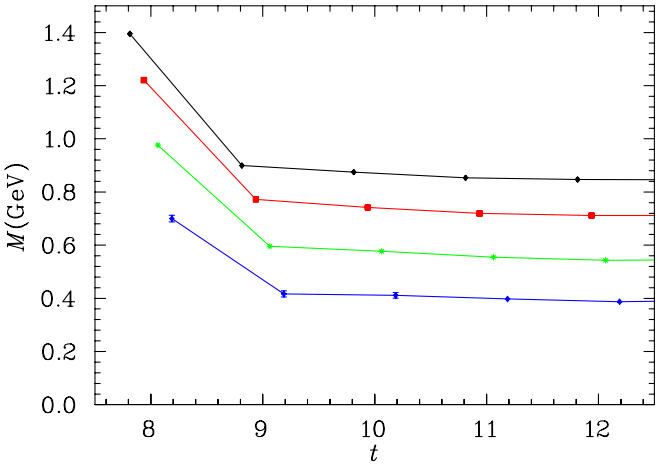

FIG. 5 (color online). Effective mass for the pseudoscalar pion interpolator $\bar{q}\gamma_5 q$.

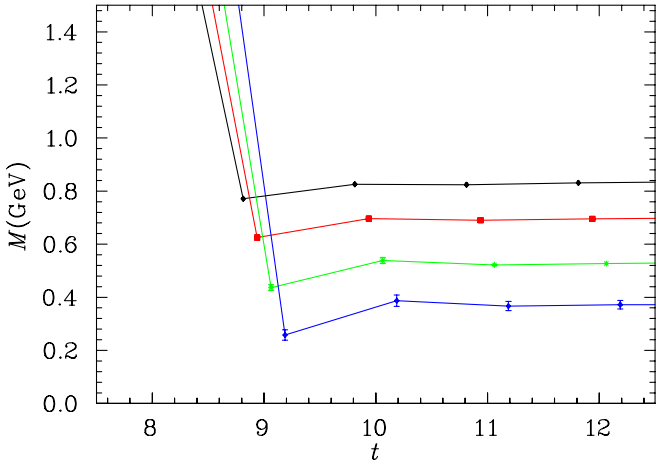

FIG. 6 (color online). Effective mass for the axial-vector pion interpolator $\bar{q}\gamma_5\gamma_4 q$.

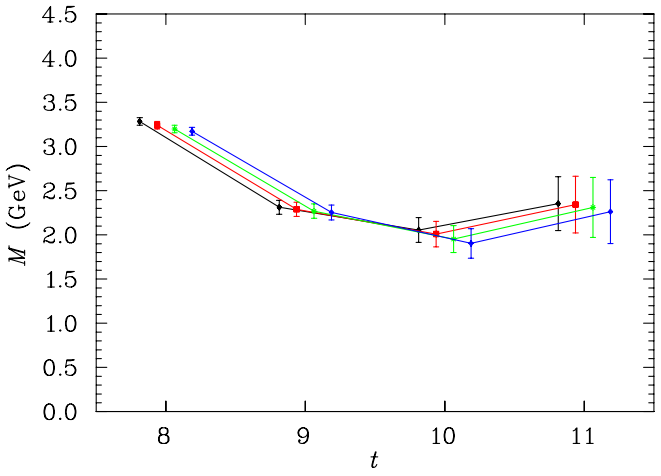

FIG. 7 (color online). Effective mass for the interpolator χ_2 with a strange quark.

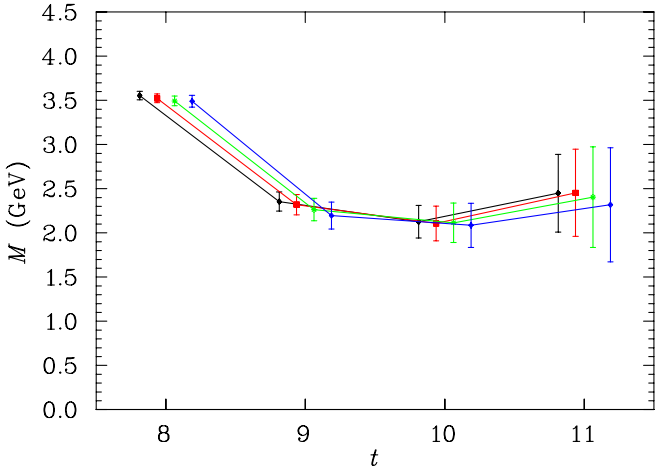

FIG. 8 (color online). As for Fig. 7, but for interpolator χ_3.

TABLE II. 1^{-+} Exotic meson mass m (GeV) vs square of pion mass m_π^2 (GeV^2).

m_π^2	χ_2 fit 10–11		χ_2 fit 10–12		χ_3 fit 10–11	
	m	χ^2/dof	m	χ^2/dof	m	χ^2/dof
0.693(3)	2.15(12)	0.69	2.16(11)	0.44	2.20(15)	0.45
0.595(4)	2.11(12)	0.77	2.12(11)	0.51	2.18(16)	0.46
0.488(3)	2.07(12)	0.85	2.08(12)	0.59	2.15(17)	0.41
0.381(3)	2.01(12)	0.91	2.03(12)	0.65	2.14(19)	0.29
0.284(3)	1.97(13)	0.78	1.98(13)	0.55	2.27(29)	0.00012
0.215(3)	1.92(14)	0.78	1.92(14)	0.40	2.25(31)	0.02
0.145(3)	1.85(17)	0.57	1.84(17)	1.76	2.26(37)	0.02
0.102(4)	1.80(23)	0.13	1.75(23)	3.04	2.46(58)	0.03

of γ_4 in the pion interpolators is to change the sign with which the large-large and small-small spinor components are combined. We also present results for the strangeness ± 1 analogue of the 1^{-+} in Figs. 7 and 8.

Table II summarizes our results for the mass of the 1^{-+} meson, with the squared pion mass provided as a measure of the input quark mass. Table III summarizes our results for the mass of the strangeness ± 1, $J^P = 1^-$ meson. The agreement observed in the results obtained from the two different 1^{-+} hybrid interpolators provides evidence that a genuine ground-state signal for the exotic has been observed.

Finally, in Fig. 9 we summarize a collection of results for the mass of 1^{-+} obtained in lattice QCD simulations thus far. The current results presented herein are compared with results from the MILC [11,16] and SESAM [12] Collaborations, both of which provide a consistent scale via r_0.

Our results compare favorably with earlier work at large quark masses. Agreement within one sigma is observed for all the quenched simulation results illustrated by filled symbols. It is interesting that the dynamical Wilson fermion results of the SESAM Collaboration [12] tend to sit somewhat higher as this is a well-known effect in baryon spectroscopy [18–20,34].

TABLE III. Strangeness ± 1, 1^- Meson mass m (GeV) vs square of pion mass m_π^2 (GeV^2).

m_π^2	χ_2 fit 10–11		χ_2 fit 10–12		χ_3 fit 10–11	
	m	χ^2/dof	m	χ^2/dof	m	χ^2/dof
0.693(3)	2.11(12)	0.76	2.12(11)	0.51	2.17(16)	0.44
0.595(4)	2.09(12)	0.81	2.10(12)	0.55	2.16(16)	0.44
0.488(3)	2.07(12)	0.85	2.08(12)	0.59	2.15(17)	0.41
0.381(3)	2.04(12)	0.88	2.05(12)	0.63	2.15(18)	0.36
0.284(3)	2.01(13)	0.85	2.02(12)	0.63	2.25(20)	0.22
0.215(3)	1.99(13)	0.87	2.00(12)	0.64	2.11(20)	0.29
0.145(3)	1.97(13)	0.73	1.97(13)	0.54	2.12(22)	0.11
0.102(4)	1.96(14)	0.56	1.96(14)	0.39	2.09(24)	0.01

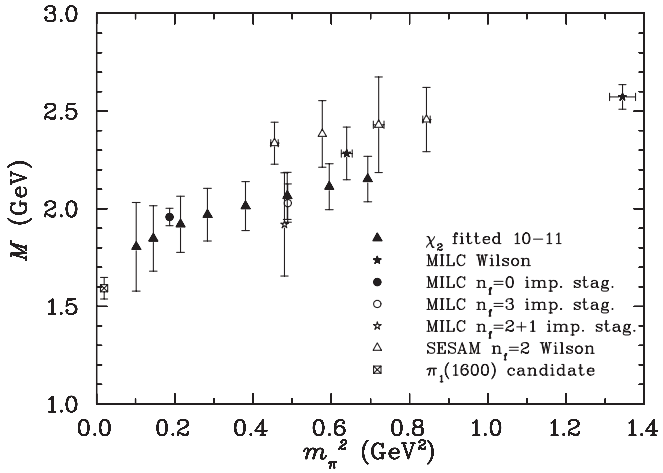

FIG. 9. A survey of results in this field. The MILC results are taken from [11] and show their $Q^4, 1^{-+} \rightarrow 1^{-+}$ results, fitted from $t = 3$ to $t = 11$. Open and closed symbols denote dynamical and quenched simulations, respectively.

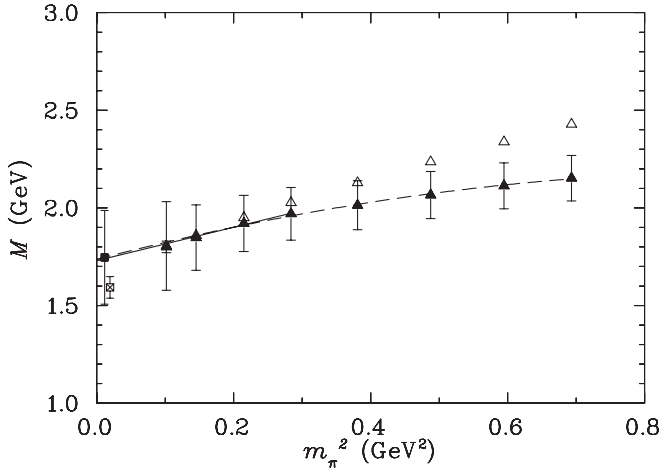

FIG. 10. The 1^{-+} exotic meson mass obtained from fits of the effective mass of the hybrid interpolator χ_2 from $t = 10 \rightarrow 12$ (full triangles) are compared with the $a_1\eta'$ two-particle state (open triangles). The extrapolation curves include a quadratic fit to all eight quark masses (dashed line) and a linear fit through the four lightest quark masses (solid line). The full square is the result of linear extrapolation to the physical pion mass, while the open square (offset for clarity) indicates the $\pi_1(1600)$ experimental candidate.

V. PHYSICAL PREDICTIONS

In comparing the results of quenched QCD simulations with experiment, the most common practice is to simply extrapolate the results linearly in m_q or m_π^2 to the physical values. However, such an approach provides no opportunity to account for the incorrect chiral nonanalytic behavior of quenched QCD [34–37].

Unfortunately, little is known about the chiral nonanalytic behavior of the 1^{-+} meson. Reference [38] provides a full QCD exploration of the chiral curvature to be expected from transitions to nearby virtual states and channels which are open at physical quark masses. While virtual channels act to push the lower-lying single-particle 1^{-+} state down in mass, it is possible to have sufficient strength lying below the 1^{-+} in the decay channels such that the 1^{-+} mass is increased [39,40]. Depending on the parameters considered in Ref. [38] governing the couplings of the various channels, corrections due to chiral curvature are estimated at the order of $+20$ to -40 MeV.

Generally speaking, chiral curvature is suppressed in the quenched approximation. For mesons, most of the physically relevant diagrams involve a sea-quark loop and are therefore absent [40,41]. However, the light quenched η' meson can provide new nonanalytic behavior, with the lowest order contributions coming as a negative-metric contribution through the double-hairpin diagrams. Not only do these contributions alter the 1^{-+} mass through self-energy contributions, but at sufficiently light quarks masses, open decay channels can dominate the two-point correlator and render its sign negative.

For the quenched 1^{-+} meson, the $a_1\eta'$ channel can be open. Using the pion mass as the η' mass a direct calculation of the mass of an $a_1\eta'$ two-particle state indicates that the 1^{-+} hybrid lies lower than the two-particle state for heavy input quark mass. This indicates that the hybrid interpolator is effective at isolating a single-particle bound state as opposed to the two-particle state at heavy quark masses. This is particularly true for the case here, where long Euclidean time evolution is difficult.

As the light quark mass regime is approached, the trend of the one and two-particle states illustrated in Fig. 10, suggests that they either merge or cross at our second lightest quark mass, such that the exotic 1^{-+} may be a resonance at our lightest quark mass and at the physical quark masses. We note that the exotic 1^{-+} mass displays the common resonance behavior of becoming bound at quark masses somewhat larger than the physical quark masses. This must happen at sufficiently heavy quark masses by quark counting rules, i.e. $2q \rightarrow 4q$ for the 1^{-+} to $a_1\eta'$ transition.

One might have some concerns about $a_1\eta'$ contaminations in the two-point correlation function affecting the extraction of the 1^{-+} meson mass [42]. However we can already make some comments.

Under the assumption that the coupling to the quenched $a_1\eta'$ channel comes with a negative metric, as suggested by chiral perturbation theory arguments, and from the observation that our correlation functions are positive, then it would appear that our interpolators couple weakly to the decay channel. Furthermore, at heavy quark masses the correlation function is dominated by the 1^{-+} bound state already at early Euclidean times suggesting that coupling to the decay channel is weak.

Thus we conclude that the hybrid interpolating fields used to explore the 1^{-+} quantum numbers are well suited to isolating the single-particle 1^{-+} exotic meson.

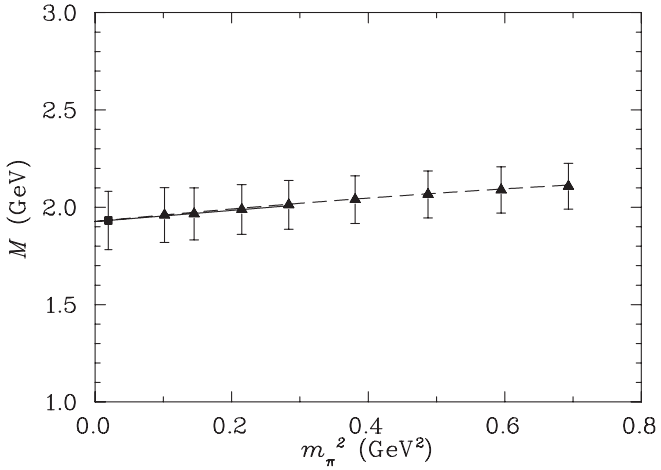

FIG. 11. Extrapolation of the associated strangeness ± 1 $J^P = 1^-$ state obtained from χ_2. Symbols are as in Fig. 10.

Moreover, since the mass of the $a_1\eta'$ channel is similar or greater than the single-particle 1^{-+} state, one can conclude that the double-hairpin $a_1\eta'$ contribution to the self-energy of the single-particle 1^{-+} exotic meson is repulsive in quenched QCD. Since the curvature observed in Fig. 9 reflects attractive interactions, we can also conclude that quenched chiral artifacts are unlikely to be large.

Hence we proceed with simple linear and quadratic extrapolations in quark mass to the physical pion mass, with the caution that chiral nonanalytic behavior could provide corrections to our simple extrapolations the order of 50 MeV in the 1^{-+} mass [38].

Figures 10 and 11 illustrate the extrapolation of the 1^{-+} exotic and its associated strangeness ± 1 1^- state to the limit of physical quark mass. We perform the linear fit using the four lightest quark masses and fit the quadratic form to all eight masses. A third-order single-elimination jackknife error analysis yields masses of 1.74(24) and 1.74(25) GeV for the linear and quadratic fits, respectively. These results agree within 1 standard deviation with the experimental $\pi_1(1600)$ result of 1.596^{+25}_{-14} GeV, and exclude the mass of the $\pi_1(1400)$ candidate.

The associated parameters of the fits are as follows. The linear form

$$m_{1^{-+}} = a_0 + a_2 m_\pi^2,$$

yields best-fit parameters of

$$a_0 = 1.73 \pm 0.15 \text{ GeV}, \qquad a_2 = 0.85 \pm 0.35 \text{ GeV}^{-1}.$$

The quadratic fit, with formula

$$m_{1^{-+}} = a_0 + a_2 m_\pi^2 + a_4 m_\pi^4,$$

returns parameters

$$a_0 = +1.74 \pm 0.15 \text{ GeV},$$
$$a_2 = +0.91 \pm 0.39 \text{ GeV}^{-1},$$
$$a_4 = -0.46 \pm 0.35 \text{ GeV}^{-3}.$$

VI. CONCLUSION

We have found a compelling signal for the $J^{PC} = 1^{-+}$ exotic meson , from which we can extrapolate a physical mass of 1.74(24) GeV. Thus for the first time in lattice studies, we find a 1^{-+} mass in agreement with the $\pi_1(1600)$ candidate.

The χ_2 interpolating field appears to be extremely useful for avoiding contamination from the $a_1\eta'$ channel, and thus is an excellent choice for this kind of study.

We have also presented the first results for a strangeness ± 1 partner of the exotic 1^{-+} meson lying at 1.92(15) GeV.

Looking forward, it will be important to quantify the effects of the quenched approximation. We plan to revisit these calculations at some future point using full dynamical FLIC fermions [43,44]. Of particular interest will be the extent to which the curvature observed in approaching the chiral regime is preserved in full QCD.

Additionally, we intend to explore the dependence of the exotic signal on the nature of the fermion source. Whilst the rapidity with which we establish a plateau in our effective mass plots suggests that our current fermion operator smearing is near optimal for isolating the ground state, it might be possible to reduce the statistical errors through a careful selection of parameters coming out of a systematic exploration of the parameter space.

Finally, a detailed finite volume analysis should be performed in order to further explore the role of the two-body decay channel.

ACKNOWLEDGMENTS

We thank Doug Toussaint for sharing his collection of results for the 1^{-+}. We thank the Australian Partnership for Advanced Computing (APAC) and the Australian National Computing Facility for Lattice Gauge Theory managed by the South Australian Partnership for Advanced Computing (SAPAC) for generous grants of supercomputer time which have enabled this project. This work was supported by the Australian Research Council.

[1] D. Alde *et al.* (IHEP-Brussels-Los Alamos-Annecy (LAPP) Collaboration), Phys. Lett. B **205**, 397 (1988).

[2] S. F. Tuan, T. Ferbel, and R. H. Dalitz, Phys. Lett. B **213**, 537 (1988).

[3] Y. D. Prokoshkin and S. A. Sadovsky, Yad. Fiz. **58N4**, 662 (1995) [Phys. At. Nucl. **58**, 606 (1995)].

[4] S. Godfrey and J. Napolitano, Rev. Mod. Phys. **71**, 1411 (1999).

[5] S. U. Chung *et al.* (E852 Collaboration), Phys. Rev. D **60**, 092001 (1999).

[6] M. Lu *et al.* (E852 Collaboration), Phys. Rev. Lett. **94**, 032002 (2005).

[7] A. R. Dzierba, R. Mitchell, A. P. Szczepaniak, M. Swat, and S. Teige, hep-ex/0502022.

[8] GlueX Website [http://www.gluex.org], and references therein.

[9] S. Eidelman *et al.* (Particle Data Group), Phys. Lett. B **592**, 1 (2004).

[10] P. Lacock, C. Michael, P. Boyle, and P. Rowland (UKQCD Collaboration), Phys. Rev. D **54**, 6997 (1996).

[11] C. W. Bernard *et al.* (MILC Collaboration), Phys. Rev. D **56**, 7039 (1997).

[12] P. Lacock and K. Schilling (TXL collaboration), Nucl. Phys. B, Proc. Suppl. **73**, 261 (1999).

[13] R. Sommer, Nucl. Phys. **B411**, 839 (1994).

[14] G. S. Bali *et al.* (TXL Collaboration), Phys. Rev. D **62**, 054503 (2000).

[15] Z. H. Mei and X. Q. Luo, Int. J. Mod. Phys. A **18**, 5713 (2003).

[16] C. Bernard *et al.*, Nucl. Phys. B, Proc. Suppl. **119**, 260 (2003).

[17] C. Michael, hep-ph/0308293.

[18] J. M. Zanotti *et al.* (CSSM Lattice Collaboration), Phys. Rev. D **65**, 074507 (2002).

[19] J. M. Zanotti *et al.*, Nucl. Phys. B, Proc. Suppl. **109A**, 101 (2002).

[20] J. M. Zanotti, B. Lasscock, D. B. Leinweber, and A. G. Williams, Phys. Rev. D **71**, 034510 (2005).

[21] S. Boinepalli, W. Kamleh, D. B. Leinweber, A. G. Williams, and J. M. Zanotti, Phys. Lett. B **616**, 196 (2005).

[22] S. Gusken, Nucl. Phys. B, Proc. Suppl. **17**, 361 (1990).

[23] J. M. Zanotti, D. B. Leinweber, A. G. Williams, J. B. Zhang, W. Melnitchouk, and S. Choe, Phys. Rev. D **68**, 054506 (2003).

[24] M. Falcioni, M. L. Paciello, G. Parisi, and B. Taglienti, Nucl. Phys. **B251**, 624 (1985); M. Albanese *et al.* (APE Collaboration), Phys. Lett. B **192**, 163 (1987).

[25] S. O. Bilson-Thompson, D. B. Leinweber, and A. G. Williams, Ann. Phys. (N.Y.) **304**, 1 (2003).

[26] F. D. R. Bonnet, P. Fitzhenry, D. B. Leinweber, M. R. Stanford, and A. G. Williams, Phys. Rev. D **62**, 094509 (2000).

[27] D. B. Leinweber *et al.*, Eur. Phys. J. A **18**, 247 (2003).

[28] M. Luscher and P. Weisz, Commun. Math. Phys. **97**, 59 (1985); **98**, 433(E) (1985).

[29] N. Cabibbo and E. Marinari, Phys. Lett. B **119**, 387 (1982).

[30] F. D. Bonnet, D. B. Leinweber, and A. G. Williams, J. Comput. Phys. **170**, 1 (2001).

[31] F. D. R. Bonnet, D. B. Leinweber, A. G. Williams, and J. M. Zanotti, Phys. Rev. D **65**, 114510 (2002).

[32] D. B. Leinweber, A. G. Williams, J. B. Zhang and F. X. Lee, Phys. Lett. B **585**, 187 (2004).

[33] A. Holl, A. Krassnigg, P. Maris, C. D. Roberts, and S. V. Wright, Phys. Rev. C **71**, 065204 (2005).

[34] R. D. Young, D. B. Leinweber, A. W. Thomas, and S. V. Wright, Phys. Rev. D **66**, 094507 (2002).

[35] R. D. Young, D. B. Leinweber, and A. W. Thomas, Phys. Rev. D **71**, 014001 (2005).

[36] D. B. Leinweber *et al.*, Phys. Rev. Lett. **94**, 212001 (2005).

[37] D. B. Leinweber *et al.*, Eur. Phys. J. A **24S2**, 79 (2005).

[38] A. W. Thomas and A. P. Szczepaniak, Phys. Lett. B **526**, 72 (2002).

[39] D. B. Leinweber and T. D. Cohen, Phys. Rev. D **49**, 3512 (1994).

[40] C. R. Allton, W. Armour, D. B. Leinweber, A. W. Thomas, and R. D. Young, Phys. Lett. B **628**, 125 (2005).

[41] S. R. Sharpe, Phys. Rev. D **46**, 3146 (1992); Phys. Rev. D **41**, 3233 (1990).

[42] K. F. Liu, Presentation at Lattice 2005.

[43] W. Kamleh, D. B. Leinweber, and A. G. Williams, Phys. Rev. D **70**, 014502 (2004).

[44] W. Kamleh, D. B. Leinweber, and A. G. Williams, Nucl. Phys. B, Proc. Suppl. **129**, 826 (2004).